



Does pulsed Tibetan deformation correlate with Indian plate motion changes?

Shihu Li ^{a,b,*}, Douwe J.J. van Hinsbergen ^c, Yani Najman ^b, Jing Liu-Zeng ^d,
Chenglong Deng ^{a,e,f}, Rixiang Zhu ^{a,e,f}

^a State Key Laboratory of Lithospheric Evolution, Institute of Geology and Geophysics, Chinese Academy of Sciences, Beijing 100029, China

^b Lancaster Environment Centre, Lancaster University, LA1 4YQ, Lancaster, UK

^c Department of Earth Sciences, Utrecht University, Utrecht, the Netherlands

^d State Key Laboratory of Earthquake Dynamics, Institute of Geology, China Earthquake Administration, Beijing 100029, China

^e Institutions of Earth Science, Chinese Academy of Sciences, Beijing 100029, China

^f College of Earth and Planetary Sciences, University of Chinese Academy of Sciences, Beijing 100049, China

ARTICLE INFO

Article history:

Received 28 April 2019

Received in revised form 4 February 2020

Accepted 6 February 2020

Available online 18 February 2020

Editor: J.P. Avouac

Keywords:

magnetostratigraphy
convergence rate
India-Asia collision
Tibetan Plateau
paleomagnetism

ABSTRACT

Models that aim to explain the causes of the significant Indian plate motion acceleration around 70 Ma, and the subsequent deceleration around 52 Ma predict different scenarios regarding crustal shortening of the Tibetan Plateau, which can be tested by precisely determining the timing of regional shortening events in Tibet. Here we attempt to determine this timing by presenting a high-resolution magnetostratigraphy of a ~3.5 km thick sedimentary sequence in the syn-contractual Gonjo Basin, east-central Tibet. We successfully isolated the primary remanence as confirmed by positive fold and reversal tests. Correlation to the geomagnetic polarity time scale reveals a 69–41.5 Ma age for the Gonjo Basin sedimentary succession. Average sedimentation rates indicate two episodes of enhanced sediment accumulation rate at 69–64 Ma and 52–48 Ma, which coincide with periods of vertical axis rotation recorded in the basin fill. This coincidence suggests a tectonic cause, which given regional structures we interpret as shortening pulses. Our results are similar to those from basins elsewhere in southern, central and northern Tibet, suggesting plateau-wide, synchronous shortening pulses at ~69–64 Ma and ~52–48 Ma. These pulses are synchronous with major acceleration and deceleration of India-Asia convergence rate, suggesting that both the acceleration and deceleration of India-Asia convergence may be associated with enhanced crustal deformation in Tibet, which we use to evaluate previous dynamic models explaining the Indian plate motion changes and India-Asia collision processes.

© 2020 Elsevier B.V. All rights reserved.

1. Introduction

The Tibetan Plateau and the Himalayan mountains are the largest of modern orogens caused mainly by the India-Asia collision. The collision was long thought to have started around 52–50 Ma (e.g., Patriat and Achache, 1984), which corresponds to the significant deceleration of India-Asia plate motion from >15 cm/yr to <8 cm/yr around 52–47 Ma (Patriat and Achache, 1984; Copley et al., 2010; van Hinsbergen et al., 2011, Fig. 1a) and enhanced crustal shortening and uplift of Tibet around this time (e.g., Searle et al., 1997), and therefore suggest a straightforward link between the slow-down of India, initial India-Asia collision, and deforma-

tion of Tibet (e.g., Patriat and Achache, 1984; Copley et al., 2010; Capitanio et al., 2010).

However, recent stratigraphic analyses revealed that Asian-derived sediments were already deposited on the Tethyan margin at 59 ± 1 Ma (Hu et al., 2015), and thereby constrained the onset of continental collision in the central part of Tibet occurred ~6 Myr prior to the deceleration of India-Asia convergence. This 6 Myr delay is significant: during this time subduction rates were so high (>15 cm/kyr) that ~1000 km of Indian plate lithosphere subducted between initial collision and slow-down. This suggests that not only is the dramatic slow-down not directly related to collision, initial collision also did not trigger a dramatic slow-down (e.g., van Hinsbergen et al., 2019). Within this context, it is now interesting to reassess whether the Tibetan upper crustal shortening is contemporaneous with initial collision at 59 ± 1 Ma, or whether it coincides with, and may thus be linked to the Indian

* Corresponding author at: Lancaster Environment Centre, Lancaster University, LA1 4YQ, Lancaster, UK.

E-mail address: s.li31@lancaster.ac.uk (S. Li).

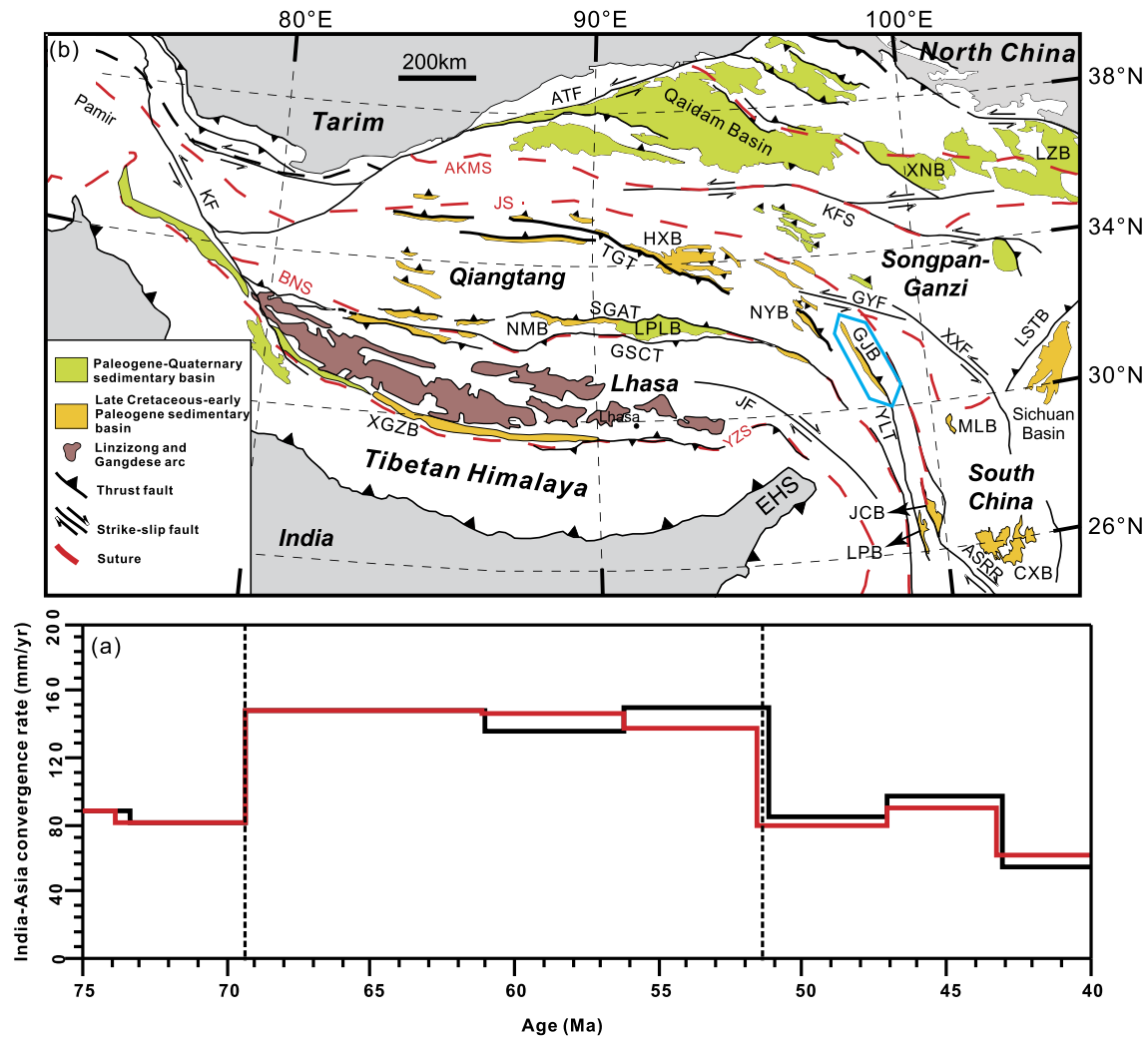


Fig. 1. (a) The India-Asia convergence rate (van Hinsbergen et al., 2011) along the two flow lines of eastern (red) and western (black) Himalaya syntaxis. (b) Simplified tectonic map of the Tibetan Plateau showing the distribution of main sedimentary basins and related strike-slip and thrust faults, and the magmatism of the Gangdese arc. The blue polygon denotes the location of the Gonjo Basin. Main abbreviations: HXB, Hoh Xil Basin; NYB, Nangqian-Yushu Basin; GJB, Gonjo Basin; XNB, Xining Basin; LZB, Lanzhou Basin; YLF, Yalong thrust fault; TGT, Tanggula thrust; EHS, Eastern Himalaya Syntaxis. (For interpretation of the colors in the figure(s), the reader is referred to the web version of this article.)

plate deceleration (and in that case, also the rapid ~70–65 Ma acceleration from ~8 cm/yr to >16 cm/yr, Fig. 1a), or neither.

The debate on the timing of collision, versus the timing of upper plate shortening, versus the timing of India-Asia plate motion changes, is thus intriguing for the first-order geodynamic questions regarding the driving mechanisms behind upper plate continental deformation as well as major plate motion changes. Plate motion changes have been explained by changes in (ridge or plume) push, (slab) pull, or (mantle) resistance against plate motion. Hypotheses for the rapid acceleration of India at ~70 Ma (Fig. 1a) include: enhanced push, exerted on India by the Deccan plume head (Cande and Stegman, 2011; van Hinsbergen et al., 2011); enhanced pull, due to the development of a hypothesized second, intra-oceanic subduction system between India and Asia since the Late Cretaceous (Jagoutz et al., 2015); or decreased resistance against Indian plate motion due to the loss of India's deep roots melted by the Deccan plume (Kumar et al., 2007), or plate interface lubrication by the arrival of Tethyan equatorial bulge sediments at the subduction trench (Behr and Becker, 2018). Deceleration of India around 52 Ma may relate to enhanced friction due to collision (e.g., Copley et al., 2010; Clark, 2012), or alternatively to resistance against lower mantle penetration of the slab (van Hinsbergen et al., 2019),

slab break-off (Zhu et al., 2015) or the termination of one of the two subduction zones (Jagoutz et al., 2015).

The hypothesis outlines contain explicit predictions for friction changes at the plate contact which may be tested through dating crustal shortening across Tibet. Enhanced push will increase friction and thus predicts enhanced shortening, whereas double subduction or plate interface lubrication predicts a decrease in friction, thus predicting no deformation changes or upper plate extension (Behr and Becker, 2018; Jagoutz et al., 2015). Therefore, determining the timing of upper plate deformation relative to plate motion changes and collision during the Late Cretaceous to Eocene may help evaluate geodynamic explanations for plate motion changes, as well as the upper plate response to continental collision.

In this paper, we attempt to evaluate whether there were discrete events in the history of Tibetan shortening during Late Cretaceous to Paleogene time. To this end, we focus on a series of sedimentary basins (Hoh Xil, Nangqian-Yushu, and Gonjo basins, Fig. 1b) with several kilometers of Late Cretaceous to Paleogene continental sediments, which are located on the Qiangtang terrane of the central Tibetan Plateau and have been shown to be controlled by basin-bounding, syn-sedimentary thrusts (Horton et al., 2002; Jin et al., 2018; Studnicki-Gizbert et al., 2008). We provide a new, high-resolution magnetostratigraphy of the Gonjo Basin in

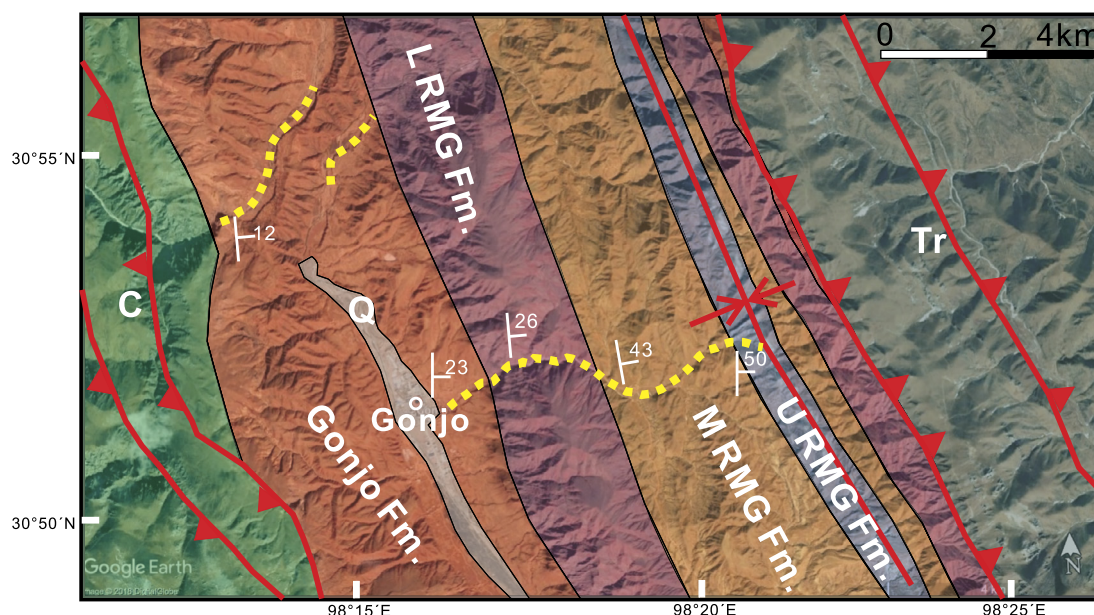


Fig. 2. Map of stratigraphy and structures of the Gonjo Basin around the Gonjo city (modified from BGMR Xizang, 1993). The dashed yellow lines refer to the magnetostratigraphic sampling sections. L/M/U RMG Fm, Lower/Middle/Upper Ranmugou Formation; C: Carboniferous; Tr: Triassic; Q: Quaternary.

the eastern Qiangtang terrane, to determine sedimentation rates through time. We test whether changes in sediment accumulation rates (SARs) may be an artifact of differences in compaction and use vertical axis rotation changes constrained by the paleomagnetic data as an independent proxy for tectonic activity. We then use our data to compare with records from other basins in central Tibet to estimate the timing of periods of enhanced regional shortening of the Tibetan Plateau, and evaluate the potential implications of our results for the causes of India-Asia plate motion changes and India-Asia collision processes.

2. Geological setting

The Gonjo Basin is located in the eastern Qiangtang terrane of east-central Tibet, close to the Eastern Himalayan Syntaxis (Fig. 1a). The basin structure is that of a basin-scale asymmetric syncline verge to the east in the footwall of the Yangla fold-thrust system. This thrust system thrusts Triassic rocks over the basin margin in the northeast and controlled the subsidence and structure of the basin (Studnicki-Gizbert et al., 2008; Tang et al., 2017; Fig. 2). Based on the presence of growth strata and the change of thickness of strata from west to east in the basin (the thickness of strata in the western limb of the syncline is significantly thicker than that in the eastern limb), Studnicki-Gizbert et al. (2008) interpreted that the Gonjo Basin was a syn-contractual basin; thrust faults initiated concurrently with the deposition of the Gonjo Basin sediments and continued after sedimentation, breaking through the original bounding folds into the basin, and forming the asymmetric syncline that we observe today (Fig. 2). Within the basin sedimentary rocks, the succession is relatively continuous and undeformed; small folds, thrust faults, and strike-slip faults which would suggest the presence of hiatus/overlap of stratigraphy and secondary structures are only developed in the core of syncline in the central part of the basin (see supplementary figure, Studnicki-Gizbert et al., 2008).

The strata in the western limb of the Gonjo Basin syncline have a thickness of >3000 m, and the strata are divided into the Gonjo Formation and the Ranmugou Formation (BGMR Xizang, 1993). The latter is further divided into three parts: lower, middle and upper Ranmugou Formation (Fig. 2). The Gonjo Formation

and the lower and middle Ranmugou Formation are dominated by red-colored mudstones, sandstones, and rare conglomerates (see supplementary figure), reflecting alluvial fan, fan-delta, floodplain and lacustrine depositional environments (Studnicki-Gizbert et al., 2008; Tang et al., 2017). In the northern part of the Gonjo Basin, a large interval (~150 m) of volcanic rocks, which consist of andesites, dacites and pyroclastics, are developed in the upper part of the middle Ranmugou Formation. The upper Ranmugou Formation consists of alternating layers of green carbonaceous shales, carbonates, and red mudstones (see supplementary figure), suggesting a lacustrine environment (Studnicki-Gizbert et al., 2008).

The original age assignment for the Gonjo Basin was Paleocene-Eocene based on limited palynological data from the upper part of the basin (BGMR Xizang, 1993). Recent isotopic dating of the volcanic rocks in the upper part of the middle Ranmugou Formation yielded an age of ~43 Ma (Studnicki-Gizbert et al., 2008; Tang et al., 2017). Detrital zircon U-Pb ages suggested a maximum age of 52.5 Ma (Zhang et al., 2018), but averaged from three samples at different depths of the strata; thus the true maximum age for the base of the sedimentary succession in the Gonjo Basin remains undefined.

3. Methods

3.1. Sampling

Paleomagnetic samples were collected around Gonjo city, where the strata of the Gonjo Basin are best exposed. The compiled section is a composite of three sub-sections with a combined stratigraphic thickness of 3325 m (Fig. 2). We correlated sub-sections according to strike; overlapped parts of the section share the same polarity suggesting our correlation between sub-sections is robust. The bedding dip of the studied section increases toward the core of the syncline from ~15° to ~60° (Fig. 2). A total of 1766 paleomagnetic samples were collected in the field with an interval of ~2 m using a gasoline-powered drill. All samples were oriented in the field with a magnetic compass. A sun-compass was also used on occasions to identify the possible local declination anomaly, which is less than 2° ($1.59 \pm 0.69^\circ$, $n = 67$), by comparing the orientation data from the two methods. All drilled cores were cut into

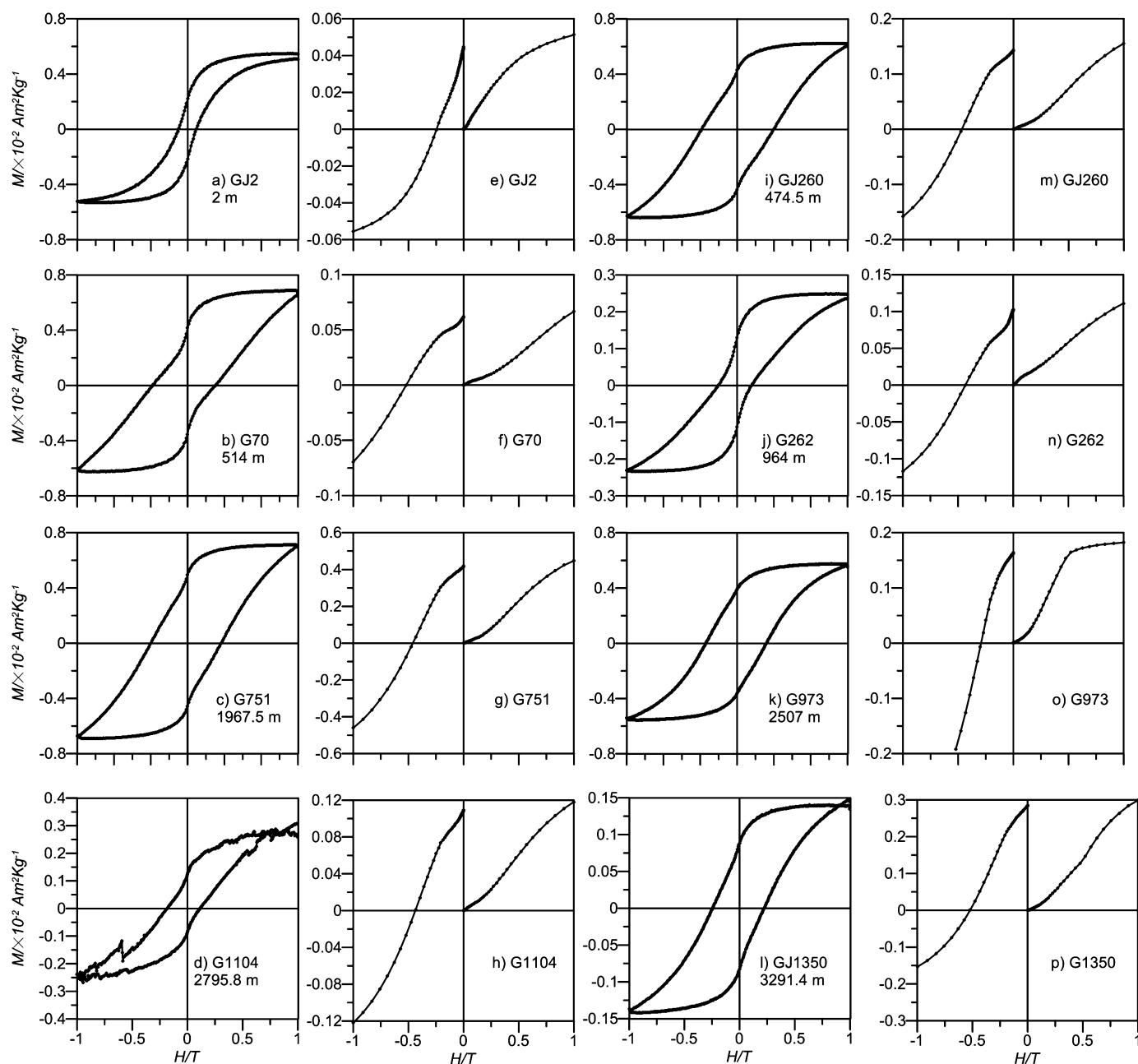


Fig. 3. (a–d, i–l) Hysteresis loops, and (e–h, m–p) IRM acquisition curves and direct current field demagnetization of the saturation IRM from representative sample of the Gonjo Basin.

1–2 specimens (2.5 cm in diameter and 2.2 cm in height) in the laboratory, remaining parts were used for rock magnetic analysis.

3.2. Paleomagnetic analysis

To identify the magnetic mineralogy in the Gonjo redbeds we measured hysteresis loops, isothermal remanent magnetization (IRM) acquisition curves, and direct current field demagnetization of the saturation IRM (SIRM) on 12 representative specimens using methods as described in Li et al. (2017a). All specimens from the Gonjo Basin were subjected to stepwise thermal demagnetization up to a maximum temperature of 690 °C, with 25–50 °C intervals below 585 °C and 10–15 °C intervals above 585 °C, using a PGL-designed PGL-100 thermal demagnetizer with internal residual magnetic field less than 5 nT. The natural remanent magnetization (NRM) was measured on a 2G Enterprises Model 760 cryogenic magnetometer inside a magnetically shielded room (<300

nT). All the measurements were conducted in the Paleomagnetism and Geochronology Laboratory (PGL) of the Institute of Geology and Geophysics, Chinese Academy of Sciences.

The principal component analysis was computed either by least-squares fits (Kirschvink, 1980) or by the great circle path (McFadden and McElhinny, 1988). The online tool set Paleomagnetism.org (Koymans et al., 2016) was employed to analyze the data.

4. Results

4.1. Paleomagnetism

The hysteresis loops are closed above a high field of 1 T, and the IRM acquisition curves are still not saturated at the maximum applied field of 1 T (Fig. 3), suggesting the dominance of high-coercivity minerals, e.g., hematite. However, the presence of

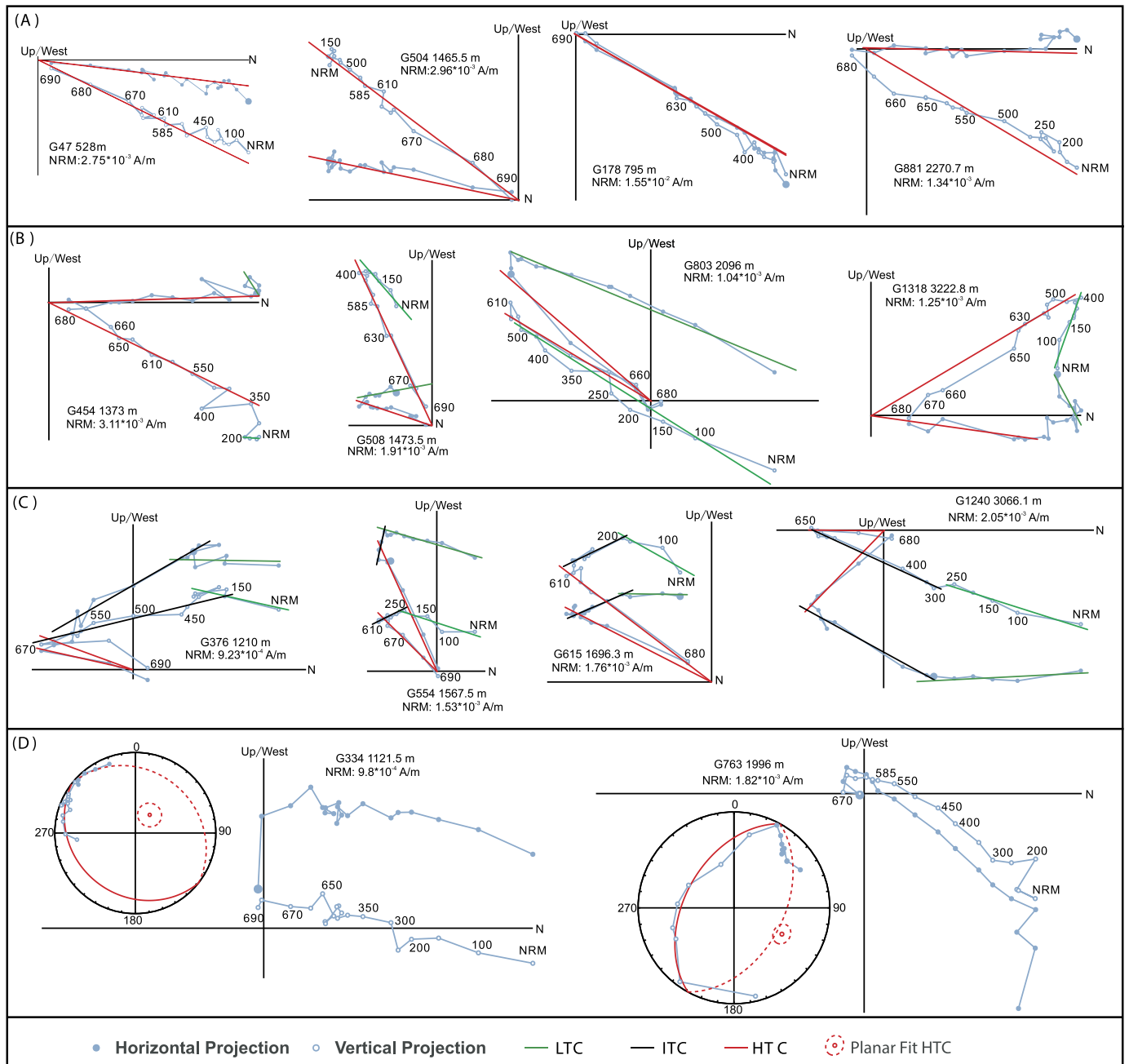


Fig. 4. Orthogonal vector projections of demagnetization for the Gonjo Basin in geographical coordinates. Solid and open symbols refer to vector projected onto the horizontal and vertical planes, respectively. NRM, natural remanent magnetization; LTC, low-temperature component; ITC, intermediate temperature component; HTC, high-temperature component.

goose-necked hysteresis loops (e.g., Fig. 3g) and rapid increase of IRM at the low field suggest the coexistence of low- (e.g., magnetite) and high-coercivity (e.g., hematite) phases (Roberts et al., 1995; Tauxe et al., 1996), which is consistent with previous paleomagnetic studies (Tong et al., 2017; Zhang et al., 2018).

As shown in Fig. 4, the demagnetization behavior of specimens from the Gonjo Basin is grouped into four types. The first type has only a single univectorial component decaying steadily toward a high temperature of 690 °C (Fig. 4a). The demagnetization diagrams of the second type show two magnetic components (Fig. 4b). A low-temperature magnetic component (LTC) was removed with varied temperatures from 300–500 °C. Above this temperature, a high-temperature magnetic component (HTC) decays linearly toward the origin and is regarded as the characteristic re-

manent magnetization (ChRM). The third type has three magnetic components (Fig. 4c). A LTC was generally removed below 300 °C, and an intermediate temperature component was mostly removed between 300 °C and 610 °C, but for some specimens as high as 650 °C (e.g., G1240, Fig. 4c). After removal of this component, a HTC was isolated until 690 °C (Fig. 4c). The ChRMs of these three types were isolated between temperatures of 610 °C and 690 °C with at least four continuous demagnetization points. A few specimens (57) show the fourth type of demagnetization behavior: the demagnetization vectors show a linear decay to the origin but move successively toward the reversed polarity on the Zijderveld diagram (Fig. 4d). When plotted on an equal-area diagram, the remanence vectors display well-defined great circle paths, suggesting that a reversed primary component is partly overprinted by a

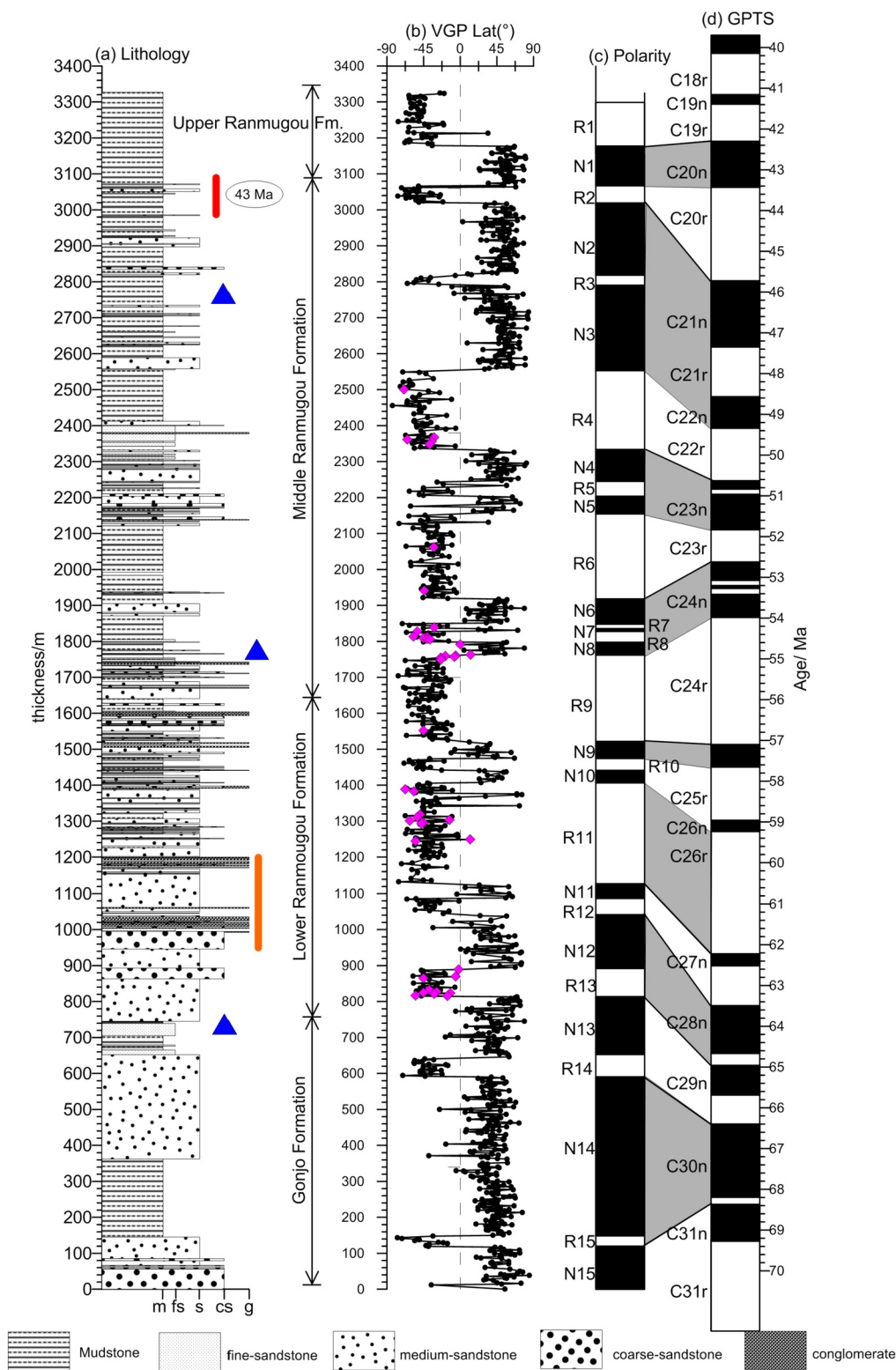


Fig. 5. Lithology (a), magnetostratigraphic (b–c) of the Gonjo Basin and their correlation with the geomagnetic polarity timescale (GPTS) (d) (Gradstein et al., 2012). Blue triangles mark the general stratigraphic position of detrital zircon U-Pb samples in Zhang et al. (2018), which were used to constrain the maximum deposition age of the Gonjo Basin. Red line denotes the stratigraphic position of the volcanic layer, which yields U-Pb (Tang et al., 2017) and $^{40}\text{Ar}/^{39}\text{Ar}$ (Studnicki-Gizbert et al., 2008) ages of ~43 Ma in the northwest Gonjo Basin. Orange line represents the position of pedogenic carbonates, which indicate a minimum average elevation of 2100–2500 m at ~60 Ma (Tang et al., 2017). The pink diamonds represent directions computed by great circle.

secondary normal component caused by overlapping blocking temperature spectra. In this case, a great circle approach was used to approximate the reversed direction based on the method of McFadden and McElhinny (1988). Directions from this type were

only used for constructing the magnetic polarity (Fig. 5, pink diamonds).

In total, 1317 specimens yielded interpretable ChRM directions, including 42 specimens analyzed by the great circle method. When

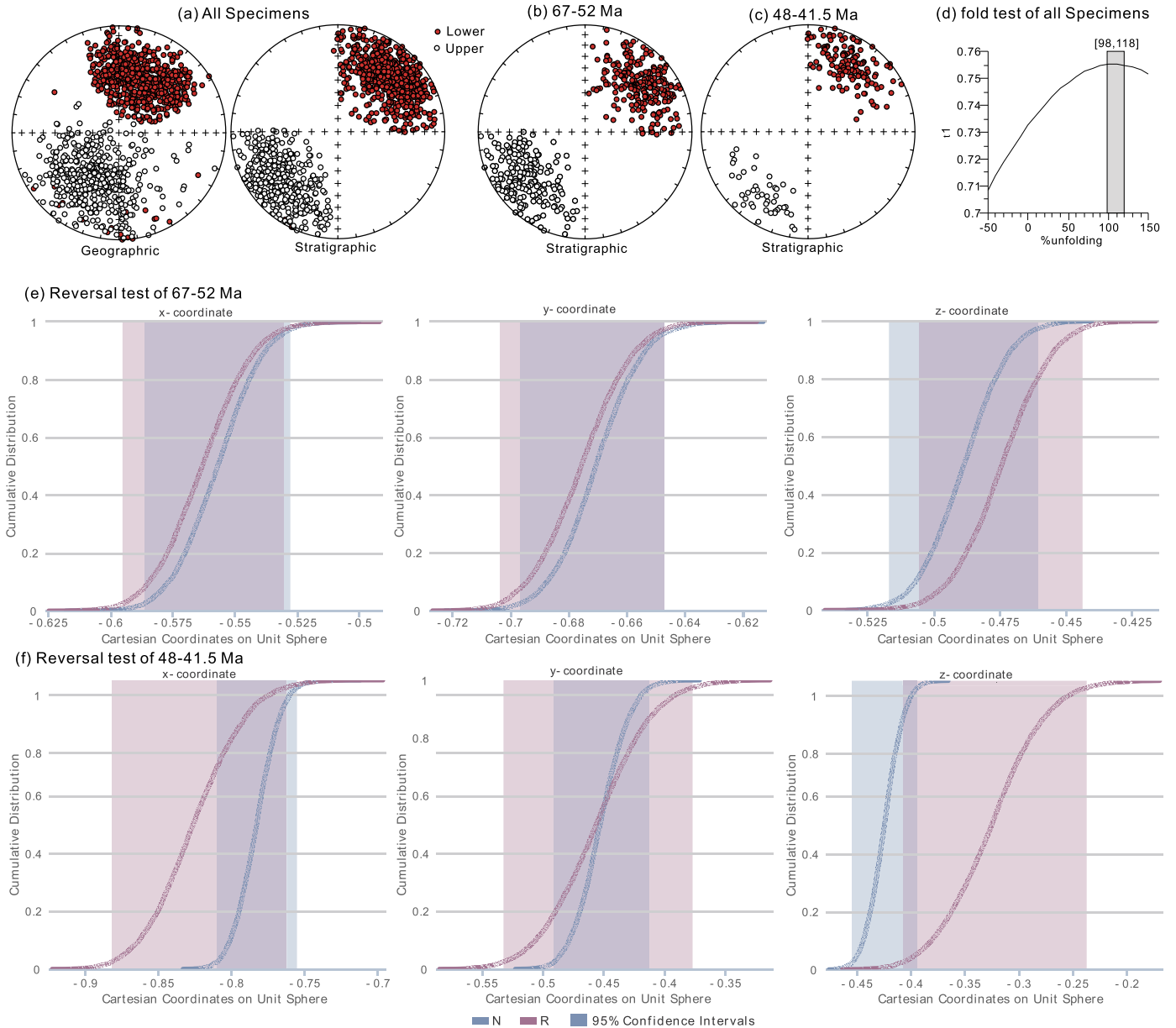


Fig. 6. Equal-area projections of (a) all the paleomagnetic directions, the non-rotated intervals of (b) 67–52 Ma and (c) 48–41.5 Ma from the Gonjo Basin. (d) Nonparametric fold tests (Tauxe and Watson, 1994) of all the paleomagnetic results. The 95% bootstrapped statistics on the first eigenvalues (τ_1) is [98, 118], indicating a positive fold test. Bootstrap reversal test (Tauxe, 2010) on results from the non-rotated interval of (e) 67–52 Ma and (f) 48–41.5 Ma. Reversed polarity directions have been inverted to their antipodes to test a common mean for the normal (blue) and reversed (purple) magnetization directions. The overlap of 95% confidence intervals for the X, Y, and Z components indicates a positive reversals test.

calculating mean directions, we excluded the 42 specimens and those specimens with north (or south) but upward (or downward) inclinations which may record the transitional behaviors of geomagnetic field. The remaining 1096 directions were grouped into 67 sites with a thickness of 50 m except the last site (see supplement Table 1 for details). Most sites typically include more than ten specimens, while site 23 was excluded because only 4 specimens are contained in this site. The plot of declination relative to age was used to constrain vertical axis rotations during deposition, which suggests a counter-clockwise rotation of $\sim 10^\circ$ from 69–67 Ma, no significant rotation between 67 and 52 Ma, $\sim 20^\circ$ clockwise rotation between 52 and 48 Ma, no rotation between 48 and 41 Ma, and $\sim 30^\circ$ clockwise rotation sometime after 41 Ma.

To examine the reliability of the paleomagnetic results, we employed a fold test on all the 1096 directions and the reversal

test on the non-rotated interval of 67–52 Ma and 48–41.5 Ma. As shown in Fig. 6, the best grouping of the overall mean directions occurs at 98%–118% (Fig. 6d), showing a positive fold test (Tauxe and Watson, 1994). Moreover, the non-rotated intervals of 67–52 Ma and 48–41.5 Ma pass a reversal test (Figs. 6e and 6f) (Tauxe, 2010). These positive field tests support a primary origin of the remanence for the Gonjo Basin.

4.2. Magnetostratigraphy

The ChRM directions were converted to virtual geomagnetic pole (VGP) latitudes to construct the magnetostratigraphy. As shown in Fig. 5, 30 magnetostratigraphic zones were identified in the studied section: 15 with normal polarity (N1–N15), and 15 with reversed polarity (R1–R15). Each polarity zone was determined using at least four paleomagnetic sampling levels.

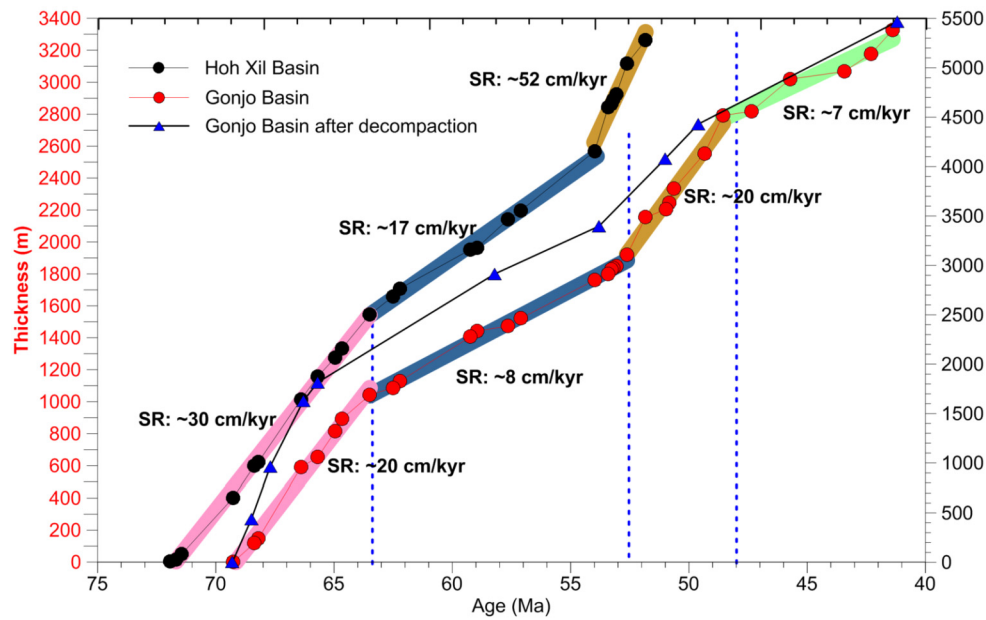


Fig. 7. Plot of magnetostratigraphic age versus stratigraphic thickness showing the variation of sediment accumulation rates of the Gonjo Basin (compacted, red dots; decompacted, blue triangle dots) and the Hoh Xil Basin (black dots, Jin et al., 2018). Note the synchronous change of sediment accumulation rates between the Gonjo Basin and the Hoh Xil Basin.

The biochronologic and geochronologic age control of the sedimentary rocks in the Gonjo Basin has been greatly improved recently. A Paleocene-Eocene age was first assigned based on limited palynological data from the upper part of the basin, such as *Palibinia* sp., *Alstonia* sp., *Carpinus* sp., *Ephedripites* and *Charites* sp. (BGMR Xizang, 1993). Studnicki-Gizbert et al. (2008) reported $^{40}\text{Ar}/^{39}\text{Ar}$ dating of volcanic rocks at the top of the middle Ranmugou Formation, which gave an average weighted age of 43.02 ± 0.23 Ma (Fig. 5). They also identified several palynomorphs from the mudstones of the upper Ranmugou Formation, such as *Momipites* sp., *Retitricolporites* sp., *Taxodiaceae* and/or *Cupressaceae*, *Inaperturites* sp., *Striatricolpites* sp., *Carya* sp., *Psilamonocolpites* sp., *Psilatricolpites* sp., *Tricolpites* sp. and *Shizosporites* sp. of which *Momipites* is regarded as common throughout the Late Eocene and Oligocene of North America (Studnicki-Gizbert et al., 2008). Later, Tang et al. (2017) carried out U-Pb zircon dating of andesite from the volcanic rock unit, which yielded a similar age of 43.2 ± 0.2 Ma to Studnicki-Gizbert et al. (2008). Although these volcanic rocks were not sampled from our section, the fold axes, strike of bedding and boundary faults, and the overall orientation of the basin are of NW-striking and in generally parallel with each other (Fig. 2), suggesting that the age of volcanic rocks in the northwestern part of the basin may be used as an age indicator in the central part of the basin by stratigraphic correlation. Moreover, Zhang et al. (2018) reported a youngest weighted mean age of 52.5 ± 1.5 Ma based on 16 zircon grains from three samples, one from the top of the Gonjo Formation, and two from the middle Ranmugou Formation (see Fig. 5 for the approximate stratigraphic locations), and concluded a maximum deposition age of 52.5 Ma for the Gonjo Basin. These lines of evidence suggest a ~ 43 Ma age for the top of the middle Ranmugou Formation and a Paleocene-Eocene age for the main part of the Ranmugou Formation.

With this age framework in mind, the correlation of our magnetic polarity zones to the global geomagnetic polarity time scale (GPTS) (Gradstein et al., 2012) is straightforward. We correlated the top normal interval of our section N1 to Chron C20n, corresponding to a time interval of 43.4–42.3 Ma. Our magnetic polarity zones are characterized by a dominance of normal polarities at the lower (N11–N15) and upper (N1–N3) parts, and reversed polarities in between (R4–R11) (Fig. 5c). This pattern of magnetozones

is similar to the GPTS of the Late Cretaceous–Middle Eocene, which shows a dominance of normal polarities in Late Cretaceous–Early Paleocene and Middle Eocene, and a dominance of reversed polarities from Late Paleocene to Early Eocene (Fig. 5d). Hence the reversed polarities of R4–R11 can be well correlated to Chrons C22r–C27r, and the normal polarities of N1–N3 and N11–N15 can be correlated to Chrons C20n–C22n and C27n–C31n, respectively (Figs. 5c and 5d). Although our observed magnetozones can be straightforwardly correlated to the GPTS, we noted that the correlation of three short reversed polarities R2, R3, and R10 to Chrons C20r, C21r, and C25r is relatively discordant, which may be caused by punctuated erosion during the transition of deposition from mudstones to sandstones (Fig. 5a). However, the erosion has only a minor effect on our magnetostratigraphic correlation, and we thus conclude that the Gonjo redbeds represent a relatively continuous depositional sequence from the Late Cretaceous (~ 69 Ma) to Middle Eocene (~ 41.5 Ma). The boundary of the Gonjo/Ranmugou formations is ca. 65.2 Ma, and the boundaries of the lower/middle and middle/upper Ranmugou formations are 55.5 Ma and 43.4 Ma, respectively.

The basal age of the Gonjo redbeds (69 Ma) seems to be much older than the youngest detrital U-Pb zircon age (52.5 ± 1.5 Ma) (Zhang et al., 2018), which normally represents the maximum depositional age of host sediments. However, the youngest detrital zircon U-Pb age in Zhang et al. (2018)'s study is an average of 16 zircon grains from three samples from different depths in the stratigraphy (see the blue triangles in Fig. 5 for stratigraphic location). The lowest sample at the top of the Gonjo Formation has two youngest zircon grains that are younger than the ~ 65 Ma age as given by our magnetostratigraphic, which seems to inconsistent with our results. However, as suggested by Dickinson and Gehrels (2009), at least three robust youngest ages are required to reliably constrain the maximum depositional age of the host rock, therefore the validity of these two zircon grains from that sample remains uncertain. Ages of the other two samples from the middle Ranmugou Formation that yield the youngest zircon grains of ~ 52 Ma are consistent with our magnetostratigraphic result.

A plot of magnetostratigraphic age versus thickness of the studied section (Fig. 7) reveals four stages of deposition with different

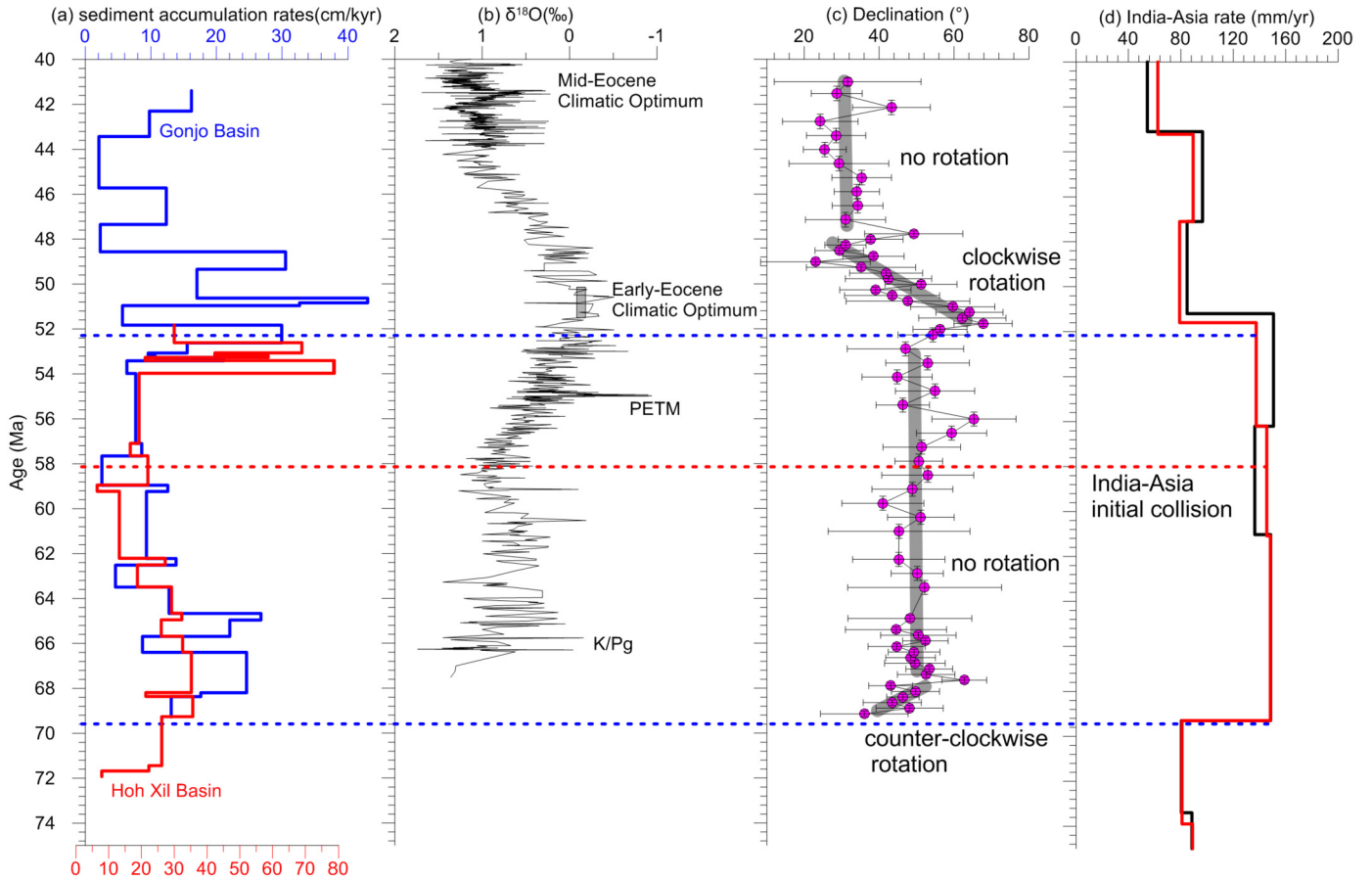


Fig. 8. Comparisons of (a) the sediment accumulation rates of the Gonjo (blue, this study) and Hoh Xil (red, Jin et al., 2018) basins, (b) stacked marine benthic oxygen-isotopic data (Zachos et al., 2008), (c) vertical axis rotations, and (d) India-Asia convergence rates (van Hinsbergen et al., 2011). Note the synchronous changes among sediment accumulation rates of the Gonjo and Hoh Xil basins, vertical axis rotations, and India-Asia convergence rates at ~70 Ma and ~52 Ma, respectively.

SARs for the Gonjo Basin: two stages of high SAR (~20 cm/kyr for 69–64 Ma and 52–48 Ma) and two stages of low SAR (~8 cm/kyr for 64–52 Ma and 48–41.5 Ma).

5. Discussion

5.1. Tectonic rotation of the eastern Tibet

The Gonjo Basin is uniquely located in the transition zone where structural trends change from east-west-oriented in the central plateau to north-south-oriented in the southeast margin of the Tibetan Plateau (Fig. 1b). The rotation history of the Gonjo Basin during the Late Cretaceous–Late Eocene therefore provides key information to address questions as to how and when this change in orientation occurred. The stratigraphically grouped 66 sites of the ChRM directions from the Gonjo Basin indicate five stages of rotation in eastern Tibet: a ~10° counter-clockwise rotation from 69 to 67 Ma, no significant rotation between 67 and 52 Ma, ~30° clockwise rotation from 52 to ~48 Ma, no significant rotation between 48 and 41 Ma, and ~30° clockwise rotation sometime after 41 Ma (Fig. 8c).

Previously, Tong et al. (2017) averaged all their paleomagnetic sites from the Gonjo Basin in one direction ($D = 35.5^\circ$, $I = 29.3^\circ$, $\alpha_{95} = 3.2^\circ$). Because of the relative rotation during deposition, this value represents a time-averaged declination, and therefore does not resolve the variation in rotation history over the Late Cretaceous to Late Eocene interval. Zhang et al. (2018) noticed varied declinations within their 61 paleomagnetic sites and identified a three-stage rotation: a clockwise rotation followed by a counter-clockwise and then another clockwise rotation, a pattern different

to our result. The difference could be simply interpreted to indicate that both Zhang et al. (2018) and our study record local rather than basin-scale regional rotation, related to the thrust architecture of the basin. However, we note that Zhang et al. (2018) did not show detailed stratigraphic and geochronologic information, or access to a continuous section. Instead they correlated two sections 30 km apart and evenly distributed their sites over a time interval of ~10 Myr that they estimated for the Gonjo Basin, which now we date to be of a duration of ~28 Myr (from 69 to 41 Ma). Therefore, the rotation pattern identified by our data, based on a continuous section and precise age constraint, is better constrained than that by Zhang et al. (2018).

The lack of rotation between 67 and 52 Ma suggests that eastern Tibet was probably dominated by laterally coherent crustal shortening during this period. The ~30° clockwise rotation between 52 and 48 Ma in the Gonjo Basin is consistent with previous paleomagnetic results from northeast and southeast Tibet (Dupont-Nivet et al., 2004; Li et al., 2017b), which also indicate that a clockwise rotation started in Eocene time (Fig. 9b). As discussed in section 5.2 below, 52 Ma marks the onset of a rapid increase in SAR of the Gonjo and Hoh Xil basins and rapid deformation in other basins from southern, central and northern Tibet, which we interpret as the onset of significant crustal shortening in the Tibetan Plateau. Therefore, the initiation of the clockwise rotation from 52 Ma reflects regionally distributed right-lateral shear between the rigid South China Block and shortening Tibetan Plateau (England and Molnar, 1990, Fig. 9b), consistent with kinematic and paleomagnetic reconstructions of Tibetan shortening and extrusion of Indochina (Li et al., 2018; van Hinsbergen et al., 2019).

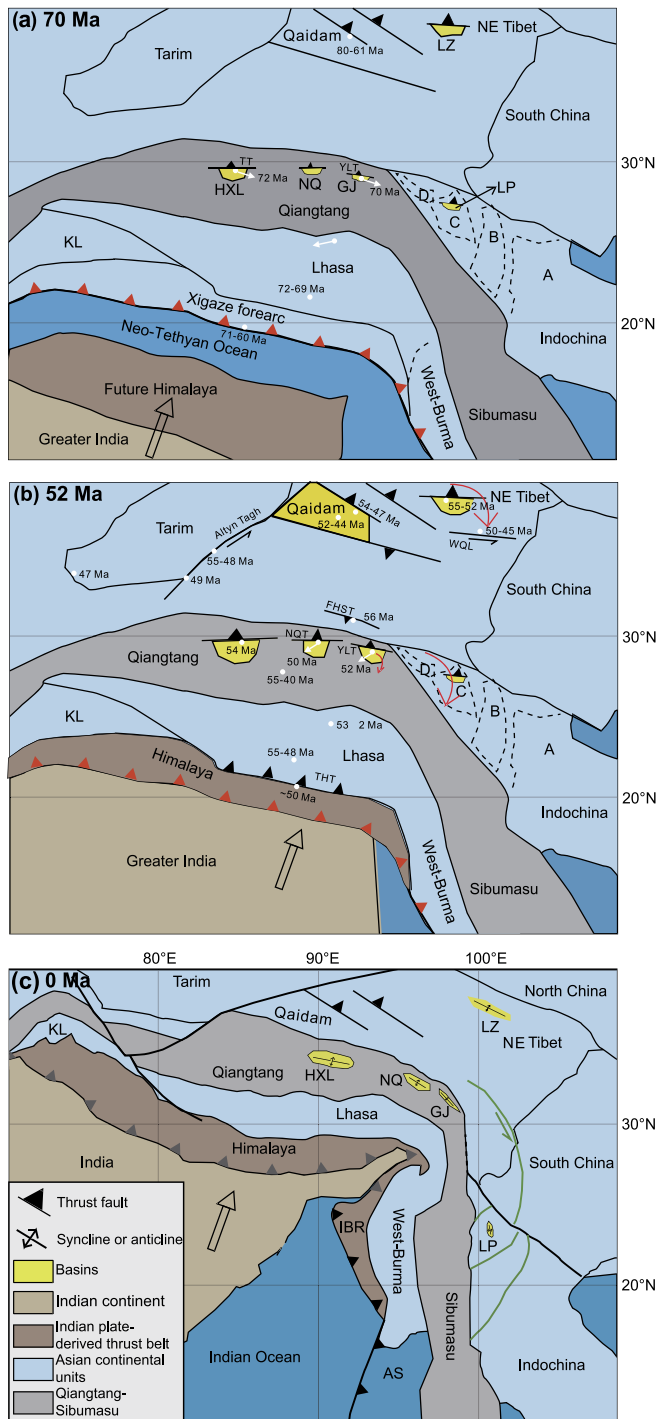


Fig. 9. Restored paleogeography map of Tibet at (a) 70 Ma, (b) 52 Ma and (c) present. (a) The rapid subduction of Neo-Tethyan at ~ 70 Ma resulted in the activation of thrust faults in central and northeast Tibet and initial deposition of a series sedimentary basins. (b) The synchronous between pulsed crustal shortening of Tibet and clockwise rotation of northeast Tibet (Dupont-Nivet et al., 2004), east Tibet (this study), and southeast Tibet (Li et al., 2017b) at ~ 52 Ma. (c) The change of geological trends and basin distribution after differential clockwise rotation. See text for the detailed discussion. The white dots and numbers denote tectonic deformation ages documented by previous studies. AS, Andaman Sea; IBR, Indo-Burman ranges; KL, Kohistan-Ladakh arc; HXL, Hoh Xil Basin; NQ, Nangqian-Yushu Basin; GJ, Gongjo Basin; LP, Lanping Basin; LZ, Lanzhou Basin; TH, Tethyan Himalaya thrust belt; FHST, Fenghuoshan thrust; NQT, Nangqian thrust; WQL: western Qinling fault. A, B, C, and D represent the four sub-terraces defined in Li et al. (2017b), including Southeast Indochina, Southern Simao, Northern Simao, and Lanping.

The coincidence between crustal shortening in Tibet and initiation of clockwise rotation in northeast, east, and southeast Tibet further suggests that upper plate deformation in Tibet at ~ 52 Ma was large enough to affect northeastern and southeastern Tibet (Dupont-Nivet et al., 2004; Li et al., 2017b), and to produce rapid and large-scale rotations of eastern Tibet.

Our previous paleomagnetic study from southeast Tibet suggested that the Qiangtang and Indochina terranes were originally a linear structure with an orientation of $N60^\circ W$ (Li et al., 2018, Fig. 9a). After a 30° clockwise rotation, the Gonjo Basin in eastern Tibet changed to $N30^\circ W$, which is consistent with the present-day strike of the Gonjo Basin (Fig. 9c). Further to the south, the southeast borderland of the Tibetan Plateau underwent as large as 60° clockwise rotation (see Li et al., 2017b and references therein), which resulted in the N-S strike of geological features observed today (Fig. 9c). Therefore, the change of geological strike from an east-west orientation in the central plateau to a north-south trend in the southeast margin of the Tibetan Plateau is mainly a consequence of different clockwise rotations from the central to southeast Tibet.

5.2. Sediment accumulation rate changes

Our new magnetostratigraphic study of the Gonjo Basin infill allows the calculation of variations in SARs. Fig. 7 shows two periods of high SAR (~ 20 cm/kyr at 69–64 Ma and 52–48 Ma) and two periods of low SAR (~ 8 cm/kyr at 64–52 Ma and 48–41.5 Ma) for the Gonjo Basin. The increase of SAR at ~ 52 Ma is coincident with an increase of coarse-grained sediments (Fig. 5a). Although our magnetostratigraphic study only represents a 1-D section of the Gonjo Basin, the uniform structures and sediments from the northwest to the southeast of the basin indicate that our 1-D velocity is likely a good approximation of 3-D volumetric SARs. In a shortening-related sedimentary basin, such variation of SARs may simply reflect timing of shortening pulses and related uplift and enhanced erosion. Alternatively, or additionally, however, such variations may be an artifact of differences in compaction or reflect climatic signals. Below, we discuss these potential contributions to the SAR changes.

We use two different methods to test whether the intervals of slow SAR are due to strong compaction. We first decompacted sediment thicknesses of the Gonjo Basin according to the observed lithologies following the methods and porosity values of Sclater and Christie (1980) using the OSXBackstrip program version 4.7 (Cardozo, 2012). This method has been successfully applied in the Xunhua Basin of northeast Tibet (Lease et al., 2012) and in the Tarim Basin of northern Tibet (Blayney et al., 2019). As shown in Fig. 7, the SAR of the Gonjo Basin after decompaction displays a similar trend as that before decompaction: two periods of high SARs (69–65.7 Ma and 53.8–49.6 Ma) alternate with two periods of relatively low SARs (65.7–53.8 Ma and 49.6–41.5 Ma), although the time of change in SARs and relative values are slightly different. This suggests that compaction plays a minor role in the SAR change.

An alternative way to evaluate the effect of compaction is through analysis of shallowing of the paleomagnetic inclination using the E/I method of Tauxe and Kent (2004), which assumes that there are strong variations in sediment compaction, whereby sediments deposited during the phases of rotation compacted much less than during intervals without rotation. The E/I method restores a measured distribution of virtual geomagnetic poles to a near-circular distribution expected from paleosecular variation in their geomagnetic field model. Sediment compaction leads to elongation of this distribution, and correcting the elongation provides an estimate for the compaction factor and restores the inclination back to the original. A prerequisite for this method is that

the source of virtual geomagnetic pole scatter is predominantly paleo-secular variation of the geomagnetic field: it is thus applicable to the parts of the section that were not deposited during rotation, i.e. the intervals with low SAR of $\sim 7\text{--}8$ cm/yr, between ~ 1200 and 1800 m, and between ~ 2600 and 3400 m (Fig. 7), but not to the intervals with high SAR of ~ 20 cm/yr that occurred during tectonic rotation. The E/I method yielded flattening factors of $0.4\text{--}0.6$ (see supplementary Table 2), which is the typical range for redbeds (e.g., Tauxe and Kent, 2004). This would recover the low SAR from $7\text{--}8$ cm/yr to $11\text{--}13$ cm/yr, which is still lower than the high compacted SAR of ~ 20 cm/yr, suggesting that the higher SARs of ~ 20 cm/yr in the intervals cannot only be explained by variations in compaction. We use the compacted SARs when comparing the Gonjo Basin with the Hoh Xil Basin to maintain consistency with them.

The SARs vary abruptly, differ by more than a factor 2, and the high SARs occur during periods of significant vertical axis rotations in the basin (Fig. 8), demonstrating regional deformation, which in this region is (oblique) shortening. It is of course possible that also climatic changes coincided with these tectonic events and contributed to the changes in SARs. Jin et al. (2018) used the global marine oxygen isotope ($\delta^{18}\text{O}$) curve (Zachos et al., 2008, Fig. 8b) as a paleoclimate reference to evaluate the potential role of climate change on the sedimentation rate change of the Hoh Xil Basin (~ 400 km west of our study area, Fig. 1), and suggested that climate change was not the dominant factor to the SAR change. However, the validity of using the oxygen isotope curve in this manner is debatable. Without detailed paleoclimate change background from Late Cretaceous-Eocene around the Tibetan Plateau, we cannot fully preclude the climate effect on the deposition of the Gonjo Basin. However, the strong temporal correlation between the increases in SAR and the timing of tectonic rotations (Fig. 8) in the shortening-controlled Gonjo Basin (Studnicki-Gizbert et al., 2008) strongly indicates that the SAR changes are dominantly tectonically-controlled. We thus interpret the high SARs record in the Gonjo Basin to reflect pulses of crustal shortening in the eastern Tibet between $\sim 69\text{--}64$ Ma, and $\sim 52\text{--}48$ Ma.

5.3. Crustal shortening of Tibet

Basins to the west on the Qiangtang terrane have similar stratigraphic records as the Gonjo Basin. The Hoh Xil Basin is the largest one in central Tibet and is controlled by the Tanggula thrust system (Jin et al., 2018) (Fig. 1a). The basin strata were recently dated at $72\text{--}51$ Ma by magnetostratigraphy and geochronology of volcanic ash (Jin et al., 2018). The Hoh Xil Basin not only has a similar structural architecture as the Gonjo Basin, but also a similar basal age (~ 70 Ma) and SAR variation pattern: a high SAR from $72\text{--}63.5$ Ma followed by a relative low SAR between 63.5 and 54 Ma, and a significant increase of SAR since 54 Ma (Fig. 7). Similarly, low-temperature thermochronology studies from the northern Qaidam Basin and central Qiangtang also suggest that northern and central Tibet underwent two stages of rapid exhumation between Late Cretaceous-Earliest Eocene and Eocene-Oligocene (Jian et al., 2018; Staisch et al., 2014, Fig. 9). To the south, in the Lhasa terrane, folded Late Cretaceous redbeds are overlain by weakly deformed Linzizong volcanics. The timing of deformation is dated between 72 Ma (Sun et al., 2012) and 69 Ma (Kapp and DeCelles, 2019). The Eocene deformation of Tibet around 52 Ma is also well documented, e.g., rapid exhumation of southern, central and northern Tibet around $\sim 55\text{--}48$ Ma as suggested by low-temperature thermochronology (Clark et al., 2010; Jian et al., 2018; and references in Li et al., 2015) and initial/rapid deposition in the Qaidam, Xining, Lanzhou, Hoh Xil and Tarim basins (see reviews in Ji et al., 2017 and Jin et al., 2018). Crustal shortening in the Lhasa terrane occurred at ~ 52 Ma has been evidenced by syn-contractional

growth strata interbedded with 53 ± 2 Ma tuffs along the northern Gangdese retroarc thrust belt (Kapp et al., 2007). Moreover, a series thrust/strike-slip faults, e.g., the Tethyan Himalaya, Fenghuoshan and Nangqian thrust faults, the left-lateral Altyn Tagh and western Qinling faults initiated/reactivated around 50 Ma (e.g., Clark et al., 2010; Jin et al., 2018; Li et al., 2015; Spurlin et al., 2005, Fig. 9b). The synchronicity of enhanced deformation in Tibet leads us to conclude that the Tibetan Plateau underwent shortening pulses at $\sim 69\text{--}64$ Ma and $\sim 52\text{--}48$ Ma.

5.4. Evaluating models explaining rapid India-Asia convergence rate changes

The SAR and deformation (rotation) pulses at $\sim 69\text{--}64$ Ma and $\sim 52\text{--}48$ Ma are synchronous with the periods of sharp acceleration and deceleration of India (Fig. 8d). If these pulses reflect shortening pulses of the Tibetan upper crust as we interpret, then both the acceleration and deceleration of India-Asia convergence appear to be associated with enhanced friction at the India-Asia plate contact. This then allows us to briefly evaluate predictions made by previous explanations for these plate convergence variations.

For the ~ 70 Ma plate acceleration and crustal deformation, enhanced friction is consistent with the prediction of a northward push of the Deccan plume head on the Indian plate (van Hinsbergen et al., 2011). Such a push would have caused acceleration of the Indian plate and accelerated the rate of Neo-Tethyan subduction and trench advance, which then may well have increased the friction between the subducting slab and overriding plate resulting in shortening in Tibet (Kapp and DeCelles, 2019) (Fig. 10a). The scenario of a second, intra-oceanic subduction zone explaining plate acceleration, as advocated by Jagoutz et al. (2015) assumed that acceleration was gradual since ~ 90 Ma, and did not explicitly address the major $70\text{--}65$ Ma acceleration. Nevertheless, the numerical modeling of the double subduction scenario predicts that the northern of the two subduction zones – below Tibet – would have the tendency to roll back (Schellart, 2005), making an enhanced friction at ~ 70 Ma difficult to explain. Finally, lubrication of the plate contact around 70 Ma, caused by the arrival of equatorial sediments in the trench, as proposed by (Behr and Becker, 2018) would predict a decrease in friction at the plate contact rather than an increase.

It is interesting to note that the central Tibet basins we studied and reviewed reveal no clear pulse of enhanced sedimentation rate, rotation, and by inference, shortening at the time of collision recorded in the Tethyan Himalaya at 59 ± 1 Ma (Hu et al., 2015), which is also supported by the $69\text{--}44$ Ma gently folded Linzizong volcanics in the Lhasa terrane (He et al., 2007). This suggests that the initial collision at 59 ± 1 Ma may just represent a soft collision, or the first phase of a two-stage collision, either an arc-India collision (Kapp and DeCelles, 2019) or a minor collision between the Tethyan microplate and Asia (van Hinsbergen et al., 2012).

The subsequent slow-down of the Indian plate at ~ 52 Ma, some $6\text{--}8$ Myr later than the time of initial collision, is however correlated with a pulse of upper plate shortening. This slow-down is classically explained by initial collision (e.g., Copley et al., 2010), but the offset between collision and slow-down, during which time up to 1000 km of India-Asia convergence occurred (e.g., Copley et al., 2010; van Hinsbergen et al., 2011), makes such an interpretation not straightforward. Alternative explanations for the 52 Ma slow-down invoke a phase of slab break-off (Zhu et al., 2015) (Fig. 10b), or slab overturning (van Hinsbergen et al., 2019) (Fig. 10c). Slab breakoff would have caused a decrease of the Indian plate's velocity due to the loss of slab pull. The rebound of the subducted Indian continental lithosphere due to its lower density relative to the mantle after slab break-off would have resulted

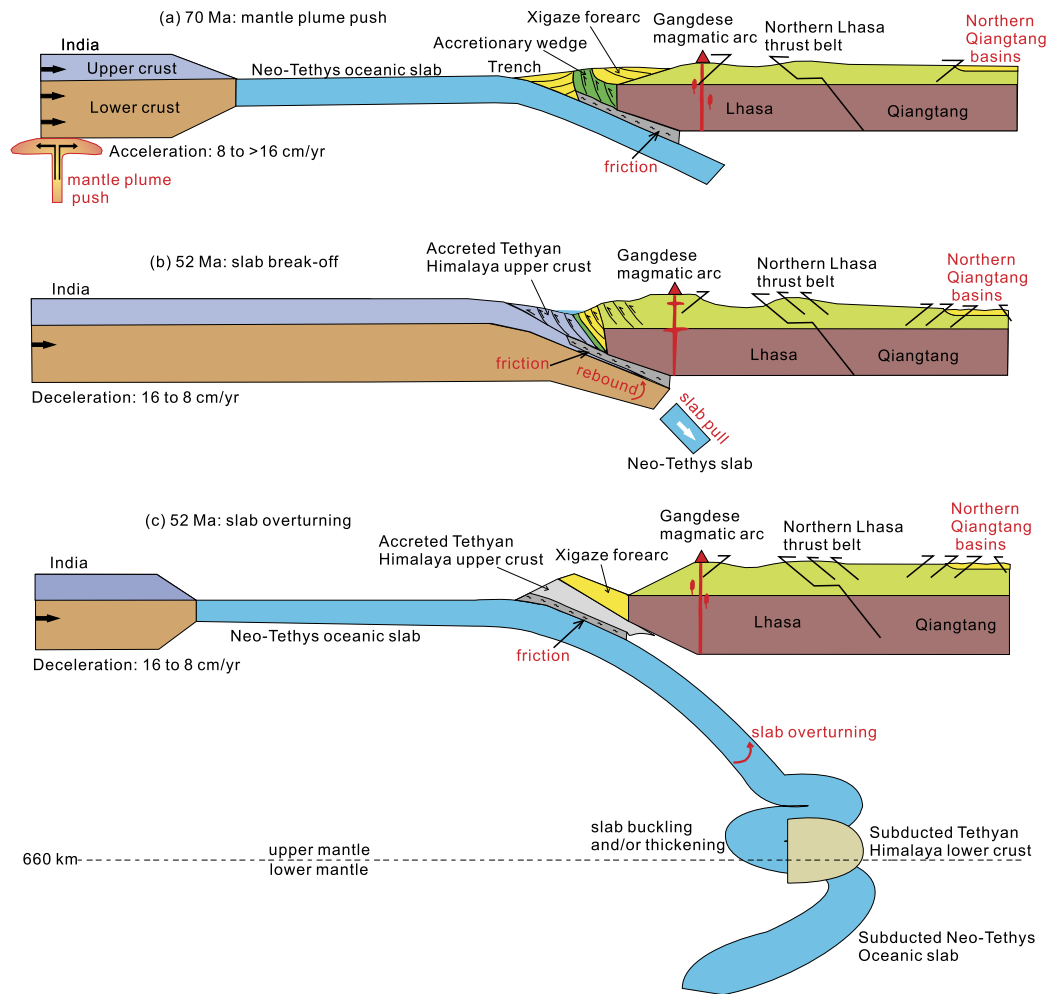


Fig. 10. Schematic models illustrating (a) the acceleration of India and increased deformation in Tibet by the push of the Deccan plume head at ~ 70 Ma, and the deceleration of India and pulse of upper plate shortening by (b) slab break-off or (c) slab overturning at ~ 52 Ma (modified after Kapp and DeCelles, 2019; Zhu et al., 2015, and van Hinsbergen et al., 2019).

in the hard collision of India with Asia, which caused upper plate shortening as demonstrated in Gonjo and related basins. The deceleration of India by the resistance of the lower mantle to the penetration of the continental lithosphere of the Tethyan Himalaya that subducted at 58 Ma, upon its arrival at the mantle transition zone. Obstruction of lower mantle penetration was proposed as an explanation why the subducting slab overturned northward, as long shown from seismic tomography (Replumaz et al., 2010). Both explanations, slab break-off or slab overturning, predict enhanced friction, consistent with our new findings.

Regardless of the exact drivers of the ~ 70 Ma acceleration and ~ 52 Ma deceleration, our study highlights the importance of, and a way towards obtaining independent constraints on the timing of upper plate deformation in Tibet. These constraints are critical to evaluate the geodynamic relationships (or absence thereof) between the continental collision, upper plate deformation, and plate kinematics.

6. Conclusions

In this study, we present a high-resolution magnetostratigraphy from the syn-contractual Gonjo Basin, eastern Tibet. Based on the magnetostratigraphy, we calculate the SAR and its temporal change in the Gonjo Basin and compare them with other basins in central Tibet and the convergence rate between India and Asia. Paleomagnetic declinations were used to constrain the rotations. With this

information, we discuss the relationship between India-Asia convergence rate and crustal shortening in the Tibetan Plateau during the India-Asia collision process. Our main conclusions are summarized as follows:

- (1) The positive fold and reversal tests suggest a primary origin of the remanence of the Gonjo Basin.
- (2) A continuous magnetostratigraphy for the Gonjo Basin reveals an age interval from 69 to 41.5 Ma.
- (3) The Gonjo Basin records two periods of rapid SAR (~ 20 cm/yr) at 69–64 Ma and 52–48 Ma and two periods of low SAR (7–8 cm/yr) at 64–52 Ma and 48–41 Ma.
- (4) Paleomagnetic declinations indicate that eastern Tibet experienced $\sim 10^\circ$ counter-clockwise at 69–67 Ma and $\sim 30^\circ$ clockwise at 52–48 Ma, followed by another $\sim 30^\circ$ clockwise rotation sometime after 41 Ma.
- (5) The two periods of rapid sedimentation are coincident with periods of vertical axis rotation, which we interpret as two pulses of crustal shortening. This result is similar to those from basins in southern, central, and northern Tibet, suggesting that these pulses occurred plateau-wide.
- (6) The crustal shortening episodes of the Tibetan Plateau correlate with a rapid acceleration and deceleration of India-Asia convergence, suggesting that both events increased friction at the India-Asia plate contact. We hypothesize that plate motion

changes, rather than initial continental collision controlled the upper plate shortening pulses of Tibet.

Declaration of competing interest

The authors declare that they have no known competing financial interests or personal relationships that could have appeared to influence the work reported in this paper.

Acknowledgements

We thank Zhongshan Shen and Jie Yuan for field assistance. Lisa Tauxe is thanked for her insightful comments on an earlier version of this paper. We are grateful for the helpful discussion with L. Ding, P. Kapp, P. DeCelles, and D. Rowley. We are grateful to the Editor, Professor Jean-Philippe Avouac, and to Professor Paul Kapp and three anonymous reviewers for their insightful suggestions. This work was funded by the Strategic Priority Research Program of the Chinese Academy of Sciences (XDA13010106) and the National Natural Science Foundation of China (41888101, 41690112, and 41761144065). S.L. acknowledges further support from the Royal Society–K.C. Wong International Fellowship NF 170033. D.J.J.v.H. acknowledges NWO Vici grant 865.17.001. R.Z. acknowledges support from the International Partnership Program (GJHZ1776) of the Chinese Academy of Sciences.

Appendix A. Supplementary material

Supplementary material related to this article can be found online at <https://doi.org/10.1016/j.epsl.2020.116144>.

References

- Behr, W.M., Becker, T.W., 2018. Sediment control on subduction plate speeds. *Earth Planet. Sci. Lett.* 502, 166–173.
- BGMZ Xizang, 1993. Regional Geology of Xizang (Tibet) Autonomous Region. Geological Memoirs Series. Geological House, Beijing.
- Blayney, T., Dupont-Nivet, G., Najman, Y., Proust, J.N., Meijer, N., Roperch, P., Sobel, E.R., Millar, I., Guo, Z., 2019. Tectonic evolution of the Pamir recorded in the western Tarim Basin (China): sedimentologic and magnetostratigraphic analyses of the Aertashi section. *Tectonics* 38 (2), 492–515.
- Cande, S.C., Stegman, D.R., 2011. Indian and African plate motions driven by the push force of the Reunion plume head. *Nature* 475, 47–52.
- Capitanio, F.A., Morra, G., Goes, S., Weinberg, R.F., Moresi, L., 2010. India–Asia convergence driven by the subduction of the Greater Indian continent. *Nat. Geosci.* 3, 136–139.
- Cardozo, N., 2012. OSX Backstrip v4.7: <http://www.ux.uis.no/~nestor/work/programs.html>.
- Clark, M.K., 2012. Continental collision slowing due to viscous mantle lithosphere rather than topography. *Nature* 483, 74–77.
- Clark, M.K., Farley, K.A., Zheng, D., Wang, Z., Duvall, A.R., 2010. Early Cenozoic faulting of the northern Tibetan Plateau margin from apatite (U–Th)/He ages. *Earth Planet. Sci. Lett.* 296, 78–88.
- Copley, A., Avouac, J.P., Royer, J.Y., 2010. India–Asia collision and the Cenozoic slowdown of the Indian plate: implications for the forces driving plate motions. *J. Geophys. Res.* 115, B03410. <https://doi.org/10.1029/2009JB006634>.
- Dickinson, W.R., Gehrels, G.E., 2009. Use of U–Pb ages of detrital zircons to infer maximum depositional ages of strata: a test against a Colorado Plateau Mesozoic database. *Earth Planet. Sci. Lett.* 288, 115–125.
- Dupont-Nivet, G., Horton, B.K., Butler, R.F., Wang, J., Zhou, J., Waanders, G.L., 2004. Paleogene clockwise tectonic rotation of the Xining–Lanzhou region, north-eastern Tibetan Plateau. *J. Geophys. Res.* 109, B04401. <https://doi.org/10.1029/2003JB002620>.
- England, P., Molnar, P., 1990. Right-lateral shear and rotation as the explanation for strike-slip faulting in eastern Tibet. *Nature* 344, 140–142.
- Gradstein, F.M., Ogg, G., Schmitz, M., 2012. The Geologic Time Scale 2012. Elsevier, Oxford, UK.
- He, S., Kapp, P., DeCelles, P.G., Heizler, G.E.G.M., 2007. Cretaceous–Tertiary geology of the Gangdese Arc in the Linzhou area, southern Tibet. *Tectonophysics* 433, 15–37.
- Horton, B.K., Yin, A., Spurlin, M.S., Zhou, J.Y., Wang, J.H., 2002. Paleocene–Eocene syncontractual sedimentation in narrow, lacustrine-dominated basins of east-central Tibet. *Geol. Soc. Am. Bull.* 114, 771–786.
- Hu, X., Garzanti, E., Moore, T., Raffi, I., 2015. Direct stratigraphic dating of India–Asia collision onset at the Selandian (middle Paleocene, 59 ± 1 Ma). *Geology* 43, 859–862.
- Jagoutz, O., Royden, L., Holt, A.F., Becker, T.W., 2015. Anomalous fast convergence of India and Eurasia caused by double subduction. *Nat. Geosci.* 8, 475–478.
- Ji, J., Zhang, K., Clift, P.D., Zhuang, G., Song, B., Ke, X., Xu, Y., 2017. High-resolution magnetostratigraphic study of the Paleogene–Neogene strata in the Northern Qaidam Basin: implications for the growth of the Northeastern Tibetan Plateau. *Gondwana Res.* 46, 141–155.
- Jian, X., Guan, P., Zhang, W., Liang, H., Feng, F., Fu, L., 2018. Late Cretaceous to early Eocene deformation in the northern Tibetan Plateau: detrital apatite fission track evidence from northern Qaidam basin. *Gondwana Res.* 60, 94–104.
- Jin, C., Liu, Q., Liang, W., Roberts, A.P., Sun, J., Hu, P., Zhao, X., Su, Y., Jiang, Z., Liu, Z., Duan, Z., Yang, H., Yuan, S., 2018. Magnetostratigraphy of the Fenghuoshan Group in the Hoh Xil Basin and its tectonic implications for India–Eurasia collision and Tibetan Plateau deformation. *Earth Planet. Sci. Lett.* 486, 41–53.
- Kapp, P., DeCelles, P.G., Leier, A.L., Fabijanic, J.M., He, S., Pullen, A., Gehrels, G.E., Ding, L., 2007. The Gangdese retroarc thrust belt revealed. *GSA Today* 17 (7). <https://doi.org/10.1130/GSAT01707A.1>.
- Kapp, P., DeCelles, P., 2019. Mesozoic–Cenozoic geological evolution the Himalayan–Tibetan orogen and working tectonic hypotheses. *Am. J. Sci.* 319 (3), 159–254.
- Kirschvink, J., 1980. The least-squares line and plane and the analysis of palaeomagnetic data. *Geophys. J. Int.* 62, 699–718.
- Koymans, M.R., Langereis, C.G., Pastor-Galán, D., van Hinsbergen, D.J.J., 2016. Paleomagnetism.org: an online multi-platform open source environment for paleomagnetic data analysis. *Comput. Geosci.* 93, 127–137.
- Kumar, P., Yuan, X., Kumar, M.R., Kind, R., Li, X., Chadha, R.K., 2007. The rapid drift of the Indian tectonic plate. *Nature* 449, 894–897.
- Lease, R.O., Burbank, D.W., Hough, B., Wang, Z., Yuan, D., 2012. Pulsed Miocene range growth in northeastern Tibet: insights from Xunhua Basin magnetostratigraphy and provenance. *Geol. Soc. Am. Bull.* 124, 657–677.
- Li, S.H., Yang, Z., Deng, C., He, H., Qin, H., Sun, L., Yuan, J., van Hinsbergen, D.J.J., Krijgsman, W., Dekkers, M.J., Pan, Y., Zhu, R., 2017a. Clockwise rotations recorded in redbeds from the Jinggu Basin of northwestern Indochina. *Geol. Soc. Am. Bull.* 129, 1100–1122.
- Li, S.H., Advokaat, E.L., van Hinsbergen, D.J.J., Koymans, M., Deng, C., Zhu, R., 2017b. Paleomagnetic constraints on the Mesozoic–Cenozoic paleolatitudinal and rotational history of Indochina and South China: review and updated kinematic reconstruction. *Earth–Sci. Rev.* 171, 58–77.
- Li, S.H., Hinsbergen, D.J.J., Deng, C., Zhu, E.L.A.R., 2018. Paleomagnetic Constraints From the Baoshan Area on the Deformation of the Qiangtang–Sibumasu Terrane Around the Eastern Himalayan Syntaxis. *J. Geophys. Res.* 123, 977–997.
- Li, Y.L., Wang, C.S., Dai, J.G., Xu, G.Q., Hou, Y.L., Li, X.H., 2015. Propagation of the deformation and growth of the Tibetan–Himalayan orogen: a review. *Earth–Sci. Rev.* 143, 36–61.
- McFadden, P., McElhinny, M., 1988. The combined analysis of remagnetization circles and direct observations in palaeomagnetism. *Earth Planet. Sci. Lett.* 87, 161–172.
- Patriat, P., Achache, J., 1984. India–Eurasia collision chronology has implications for crustal shortening and driving mechanism of plates. *Nature* 311 (5987), 615–621.
- Replumaz, A., Negredo, A.M., Guillot, S., Villaseñor, A., 2010. Multiple episodes of continental subduction during India/Asia convergence: insight from seismic tomography and tectonic reconstruction. *Tectonophysics* 483, 125–134.
- Roberts, A., Cui, Y.L., Verosub, K.L., 1995. Wasp-waisted hysteresis loops Mineral magnetic characteristics and discrimination of components in mixed magnetic systems. *J. Geophys. Res.* 100, 17909–17924.
- Schellart, W.P., 2005. Influence of the subducting plate velocity on the geometry of the slab and migration of the subduction hinge. *Earth Planet. Sci. Lett.* 231, 197–219.
- Sclater, J.G., Christie, P.A.F., 1980. Continental stretching: an explanation of the Post-Mid-Cretaceous subsidence of the central North Sea Basin. *J. Geophys. Res.* 85, 3711–3739.
- Searle, M., Corfield, R.I., Stephenson, B.E.N., McCarron, J.O.E., 1997. Structure of the North Indian continental margin in the Ladakh–Zaskar Himalayas: implications for the timing of obduction of the Spontang ophiolite, India–Asia collision and deformation events in the Himalaya. *Geol. Mag.* 134 (3), 297–316.
- Spurlin, M.S., Yin, A., Horton, B.K., Zhou, J., Wang, J., 2005. Structural evolution of the Yushu–Nangqian region and its relationship to syncontractual igneous activity east-central Tibet. *Geol. Soc. Am. Bull.* 117, 1293–1317.
- Staisch, L.M., Niemi, N.A., Hong, C., Clark, M.K., Rowley, D.B., Currie, B., 2014. A Cretaceous–Eocene depositional age for the Fenghuoshan Group, Hoh Xil Basin: implications for the tectonic evolution of the northern Tibet Plateau. *Tectonics* 33. <https://doi.org/10.1002/2013TC003367>.
- Studnicki-Gizbert, C., Burchfiel, B.C., Li, Z., Chen, Z., 2008. Early Tertiary Gonjo basin, eastern Tibet: sedimentary and structural record of the early history of India–Asia collision. *Geos.* 4, 713–735.
- Sun, Z., Pei, J.L., Li, H.B., Xu, W., Jiang, W., Zhu, Z.M., Wang, X.S., Yang, Z.Y., 2012. Palaeomagnetism of late Cretaceous sediments from southern Tibet: evidence for the consistent palaeolatitudes of the southern margin of Eurasia prior to the collision with India. *Gondwana Res.* 21, 53–63.

- Tang, M., Liu-Zeng, J., Hoke, G.D., Xu, Q., Wang, W., Li, Z., Zhang, J., Wang, W., 2017. Paleoelevation reconstruction of the Paleocene-Eocene Gonjo basin, SE-central Tibet. *Tectonophysics* 712–713, 170–181.
- Tauxe, L., Watson, G.S., 1994. The fold test: an eigen analysis approach. *Earth Planet. Sci. Lett.* 122, 331–341.
- Tauxe, L., Mullender, T.A.T., Pick, T., 1996. Potbellies, wasp-waists, and superparamagnetism in magnetic hysteresis. *J. Geophys. Res.* 101, 571–583.
- Tauxe, L., Kent, D.V., 2004. A simplified statistical model for the geomagnetic field and the detection of shallow bias in paleomagnetic inclinations: was the ancient magnetic field dipolar? In: Channell, J.E.T., Kent, D.V., Lowrie, W., Meert, J.G. (Eds.), *Timescales of the Paleomagnetic Field*. In: *Geophys. Monogr. Ser.*, vol. 145. American Geophysical Union, Washington, D.C., pp. 101–115.
- Tauxe, L., 2010. *Essentials of Paleomagnetism*. University of California Press, Berkeley, 512 pp.
- Tong, Y., Yang, Z., Mao, C., Pei, J., Pu, Z., Xu, Y., 2017. Paleomagnetism of Eocene red-beds in the eastern part of the Qiangtang Terrane and its implications for uplift and southward crustal extrusion in the southeastern edge of the Tibetan Plateau. *Earth Planet. Sci. Lett.* 475, 1–14.
- van Hinsbergen, D.J.J., Steinberger, B., Doubrovine, P.V., Gassmüller, R., 2011. Acceleration and deceleration of India-Asia convergence since the Cretaceous: roles of mantle plumes and continental collision. *J. Geophys. Res.* 116, B06101. <https://doi.org/10.1029/2010JB008051>.
- van Hinsbergen, D.J.J., Lippert, P.C., Dupont-Nivet, G., McQuarrie, N., Doubrovine, P.V., Spakman, W., Torsvik, T.H., 2012. Greater India Basin hypothesis and a two-stage Cenozoic collision between India and Asia. *Proc. Natl. Acad. Sci. USA* 109, 7659–7664.
- van Hinsbergen, D.J.J., Lippert, P.C., Li, S., Huang, W., Advokaat, E.L., Spakman, W., 2019. Reconstructing Greater India: paleogeographic, kinematic, and geodynamic perspectives. *Tectonophysics* 760, 69–94.
- Zachos, J.C., Dickens, G.R., Zeebe, R.E., 2008. An early Cenozoic perspective on greenhouse warming and carbon-cycle dynamics. *Nature* 451, 279–283.
- Zhang, Y., Huang, W., Huang, B., van Hinsbergen, D.J.J., Yang, T., Dupont-Nivet, G., Guo, Z., 2018. 53–43 Ma deformation of the Eastern Tibet revealed by three stages of tectonic rotation in the Gongjue basin. *J. Geophys. Res.* 123, 3320–3338.
- Zhu, D.C., Wang, Q., Zhao, Z.D., Chung, S.L., Cawood, P.A., Niu, Y., Liu, S.A., Wu, F.Y., Mo, X.X., 2015. Magmatic record of India-Asia collision. *Sci. Rep.* 5, 14289.